Effect of exciton-carrier thermodynamics on the GaAs quantum well photoluminescence

H. W. Yoon,* D. R. Wake, and J. P. Wolfe
Frederick Seitz Materials Research Laboratory, University of Illinois at Urbana-Champaign, Urbana, Illinois 61801
(Received 16 January 1996)

In order to explain the power-dependent temporal behavior of the photoluminescence from free excitons in a GaAs quantum well following a short optical pulse, we consider the excitons and free carriers to be a nearly ideal gas in thermodynamic equilibrium. The temperature of the gas, which decreases in time after the pulse due to cooling by phonon emission, can be measured experimentally from the free-carrier recombination luminescence. Because only excitons with near-zero kinetic energy can luminesce, the photoluminescence intensity depends on the excitonic-gas temperature. Due to the law of mass action between excitons and free carriers, the photoluminescence intensity of excitons also depends on the density of the gas, which decays in time. Using the known binding energy of excitons, we find that the density-dependent temporal behavior of the photoluminescence is consistent with a simple thermodynamic equilibrium between excitons and free carriers. [S0163-1829(96)11527-7]

INTRODUCTION

Excitons in quantum wells, as a consequence of their two-dimensional confinement, have increased binding energies and enhanced oscillator strengths compared to excitons in bulk materials. In GaAs quantum wells, the most prominent features seen in the optical spectra arise from excitonic effects, and many spectroscopic studies have been conducted to determine the homogeneous linewidths, the intrinsic lifetimes, and excitonic ionization times, for example. Past studies of the time dynamics of excitons can be broadly categorized into resonant and nonresonant excitation studies, since they probe different properties of excitons. Under conditions of resonant excitation and low temperature ($\leqslant 2$ K), the dynamics of excitons have been shown to be governed by spin and momentum relaxation of excitons.[1] However, under conditions of nonresonant excitation and high temperatures, the exciton temporal dynamics are different, since spin splitting is not important and the kinetic energy of excitons can be comparable to the Coulombic binding energy of excitons. Despite the numerous studies of excitons using photoluminescence (PL) spectroscopy,[2,3,5,6] the ''gas kinetics'' (e.g., interconversion) of excitons and free carriers, and its effect on the time dynamics of the exciton PL intensity, have not been described. In this paper we show that significant changes in the decay of excitonic PL as a function of density and excitation energy can be understood in terms of a thermodynamic equilibrium between excitons and carriers.

Past studies with time-resolved PL have shown that the thermal ionization of excitons into electrons and holes should be considered in any description of exciton PL.[3] Excitation with photon energies greater than the band-gap energy leads to the formation of carriers with temperatures greater than the lattice temperatures; indeed, the initial thermal energies of carriers can greatly exceed the exciton binding energy. Carrier temperatures have been measured from the energy dependence of the PL associated with band-to-band recombination of free electrons and holes. At sufficient densities it is reasonable that the exciton temperature is equal to the measured carrier temperature because interparticle scattering times are much shorter than the thermal relaxation times.[4]

In a practical sense, the principal aim of our present study is to understand the behavior of the time-resolved exciton PL intensity with varying excitation energy and density. Such observations bear directly on the kinetics of the photoexcited particles. Consistent with earlier studies,[5] we have found, that after a short pulse, the time delay to the peak of the excitonic-PL intensity increases with excitation power. This effect is illustrated for our sample in Fig. 1. Such changes in the exciton PL have been empirically characterized by a rise time t_r, which is defined as the time interval between the excitation pulse and the time of the highest PL intensity. The rise time was found to depend upon the ''excess energy'' given to the photoexcited pairs by the laser, defined by $\Delta E = \hbar\omega_{\text{laser}} - E_{\text{HH}}$, with $\hbar\omega_{\text{laser}}$ the incident photon energy and E_{HH} the band-bottom energy for the heavy-hole excitons. The study by Kusano *et al.*[5] found $t_r = 150$ ps for near-resonant excitation with an excess energy of $\Delta E = 5$ meV, and an increase in the rise time to $t_r = 400$ ps with an

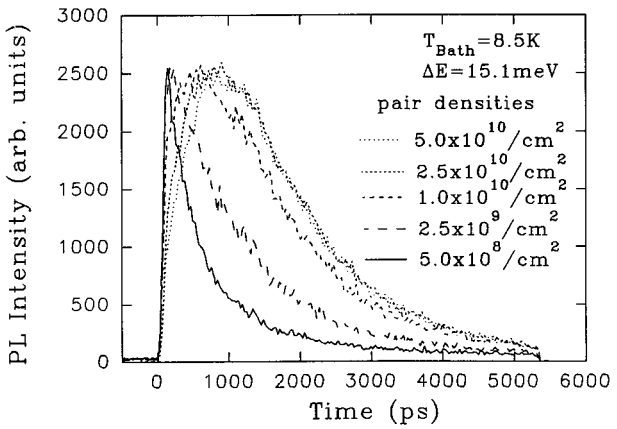

FIG. 1. Time-resolved heavy-hole exciton PL at $T_{\text{Bath}} = 8.5$ K, with excitation at 15.1 meV above the heavy-hole exciton energy. Shown are PL intensities for various excitation densities ranging from $5\times10^8/\text{cm}^2$ to $5\times10^{10}/\text{cm}^2$.

increase in excess energy to $\Delta E = 30$ meV. However, a further increase in the excitation energy to $\Delta E = 150$ meV did not increase the rise time beyond 400 ps. This study also found an increase in the first moment of the temporal profile with increasing excess energy. Other experimenters have also reported increases in t_r with increasing excess energies.[6,7]

Previous reports have also shown that changes in the PL rise time occur with fixed excitation energy and varying excitation density. Eccleston *et al.*[7] reported that with 2.4-meV excess energy the rise time decreased from 150 ps at an excitation density of $10^7/\mathrm{cm}^2$ to ~ 70 ps at an excitation density of $10^{10}/\mathrm{cm}^2$. In contrast, Damen *et al.*[8] found that at excess energy of 47 meV the rise times *increased* from ~ 200 ps at $< 5\times 10^9/\mathrm{cm}^2$ to ~ 400 ps at $5\times 10^{10}/\mathrm{cm}^2$. The lack of consensus on the behavior of the rise times suggests that the temporal dynamics of the exciton PL depend crucially on the initial excitation conditions, and may also be sample dependent. In this paper we attempt to determine the factors needed to understand this density-dependent and pump-energy-dependent time evolution of the exciton PL. We aim to learn about the cooling and kinetics of the exciton gas from such studies.

Previous studies of time-resolved exciton PL have taken two different approaches. Both approaches reasonably assume that only excitons with in-plane wave vectors near $k = 0$ can radiatively decay. This assumption automatically implies that variations in the energy distribution of excitons will affect the temporal profile of the PL. In model 1, the energy levels in the excitonic system were empirically modeled by three levels.[5,6] The excitons are separated into $k \neq 0$ and $k = 0$ excitons, and excitons with $k \neq 0$ must relax to excitons with $k = 0$ before they can couple to photons. This model has two time parameters τ_r and τ_D, where τ_r is the time for the relaxation of excitons with $k \neq 0$ to relax into the $k = 0$ state, and τ_D is the time for exciton at $k = 0$ to radiatively decay. The model can account for the general features of the time-resolved exciton PL, but does not make connections between τ_r and physical parameters such as carrier density, temperature, and energy distribution.

The second model more directly related the time dependence of the excitonic PL to changes in the energy distribution of excitons.[7,8] Excitons were assumed to have a Boltzmann distribution, and only excitons within an energy width E_1 of $k = 0$ couple to photons.[9] The time evolution of the exciton luminescence intensity was described in terms of the excitonic energy distribution. Near $k = 0$ the distribution function at low temperatures has a greater value than at higher temperatures, so as the excitonic temperature cools with time, the peak of the exciton PL intensity occurs at a time later than $t = 0$, also dependent on the recombination rate.

In our work we take elements of both of the above descriptions, but we also attempt to predict the energy evolution of the excitons by considering the thermodynamics between excitons and free carriers. The thermodynamic behavior of excitonic matter has been extensively applied to semiconductors with longer excitonic lifetimes, such as electron-hole liquid in Ge and Si, and excitons in Cu_2O. The thermodynamics of excitons and excitonic molecules in Si was examined by Gourley and Wolfe.[10] More recently, evidence of the thermodynamic equilibrium of excitons and biexcitons in GaAs quantum wells has been reported.[11] In GaAs quantum wells, the temperature dependence of excitonic recombination times has been described in terms of the thermal equilibrium between excitons and free electrons and holes.[12,13] From the thermal ionization of excitons in 70-Å GaAs quantum wells excited by a helium-neon laser, Colocci, Gurioli, and Vinattieri[14] have shown that the two-dimensional law of mass action is followed from ~ 300 to 106 K. They ascertained an exciton binding energy of 12 meV from the PL data by applying the two-dimensional (2D) law of mass action, in good agreement with the calculated binding energy.

In order to determine if there is a chemical equilibrium between excitons and carriers, one must be able to measure both the carrier temperature and density at each point in time. The time-resolved carrier density is not simply related to the PL intensity if the effective volume occupied by the particles changes in time. This is a particularly important consideration when the excitation beam is focused on a small region, allowing one to obtain higher densities but also bringing particle diffusion into play: the effective volume of the excitonic gas may expand in time, and the particle density is proportional to PL intensity/volume. Only recently have studies taken into account the time-resolved *spatial* distribution of photoexcited carriers. In our present studies, we make use of our previously reported spatial transport measurements on the same sample.[15]

In addition to gas volume, we must determine the gas temperature. We find that the PL spectra consist of the free-exciton components plus recombination radiation of free electrons and holes (sometimes referred to as the ''plasma'') starting at the band-gap edge. The center of the excitonic peak is separated in energy from the band-to-band electron-hole luminescence by the exciton binding energy. We determine the carrier temperature from the high-energy slope of the electron-hole recombination spectrum. At our excitation densities, we reasonably assume that the free carriers and excitons acquire the same temperature due to rapid interparticle collisions.

The temporal decay of the carrier temperature depends on the initial pump energy, the bath temperature, and initial photon density. For excitation with photon energy in excess of the heavy-hole exciton energy (nonresonant case), we find that for $T_{\mathrm{Bath}} \geqslant 40$ K there is a rapid cooling approximately described by a time constant, $\tau \leqslant 40$ ps, which is near our instrumental resolution. For $T_{\mathrm{Bath}} < 40$ K, the carrier cooling is described by a fast ($\tau_1 \leqslant 40$ ps) component and a slow ($\tau_2 \approx 2$ ns) component. By analyzing the energy-loss rate as a function of the carrier temperatures, we infer that the fast component is due to LO-phonon emission, and that the slower cooling is associated with acoustic-phonon emission.[16]

We describe the thermodynamics of the excitonic gas in terms of a two-dimensional ideal-gas model in which the excitons exist in equilibrium with free electrons and holes.[17] We restrict the number of excitons which can emit photons[18] to an energy width E_1 near $E = 0$. We use this model along with the experimentally measured time-dependent carrier temperatures and densities to fit a representative temporal profile of the exciton PL. The calculated PL intensities de-

termined in this way are found to be weakly dependent on the magnitude of exciton binding energy, but they are strongly dependent on the carrier cooling and carrier expansion rates.

A good correspondence between the calculated exciton PL intensities and the experimentally measured intensities is found by varying the initial carrier temperatures, the carrier cooling rates, and the spatial expansion rates. We conclude that the initial carrier temperature rises as the excess energy is increased, in agreement with a previous study.[24] An increase in the initial carrier temperatures with excitation energy presumably arises from the larger excess kinetic energy of photoexcited carriers. Also, the volume expansion rates increase with increasing excess energies. At a fixed excess energy of 15.1 meV, we find that good fits of the exciton PL are achieved if the carrier cooling rates are slowed with increasing excitation density.

EXPERIMENTAL ASPECTS

The GaAs/$Al_xGa_{1-x}As$ multiple-quantum-well structure studied here consists of 30 periods of 210-Å GaAs wells and 100-Å $Al_{0.3}Ga_{0.7}As$ barriers. The GaAs substrate is removed in a 0.5-mm window by selective etching, so that absorption and PL spectra may be recorded in the same region. The sample is placed in an optical cryostat to maintain the temperature from 5 to 300 K. The excitation region is focused on a region as small as 3 μm by means of an achromatic lens inside the cryostat. For PL measurements, the optical excitation axis may be shifted laterally relative to the spectrometer optical axis by refractive displacement of the excitation beam through rotatable glass blocks at a focal point prior to entering the cryostat. Additional experimental details are discussed in Ref. 15.

Time-resolved PL measurements are obtained by excitation with a 3-ps laser pulse and detection with a Hamammatsu multichannel plate photomultiplier tube, using time-correlated photon counting. The light is dispersed by a $\frac{1}{2}$-m spectrometer with reduced mirror width, so that empirically we obtain a $\sim$36-ps time resolution. For the best spatial resolution, the luminescence is restricted by a 60-μm-diameter pinhole placed at the focal point of the collection lens, which is then reimaged onto the entrance slit of the spectrometer. The measurements of spatial expansion are taken from the previously reported results (Ref. 15). By the use of the confocal technique we are able to obtain $\sim$3-μm resolution.

CARRIER TEMPERATURES FROM BAND-TO-BAND RECOMBINATION

An important aspect of our experiments is the determination of the carrier temperature as a function of time. Since interparticle scattering leads to the establishment of a common temperature between excitons and free carriers within 1 ps at the densities used here, we use the term ''carrier temperature'' to refer to the temperature of both species.[19] The carrier temperatures are determined directly from the slope on a semilogarithmic plot of the band-to-band recombination spectra.[20]

It is not possible to measure the carrier temperatures from the heavy-hole exciton line because exciton luminescence occurs only near $k=0$. In contrast, the band-to-band recombination process in which a free electron and a hole recombine and emit a photon occurs for all values of momenta. For nondegenerate electrons and holes in a 2D potential well, the luminescence intensity for band-to-band recombination is given by[21]

$$I(\hbar\omega)\propto\alpha(\hbar\omega-E_g)f_e(\hbar\omega)f_h(\hbar\omega), \tag{1}$$

where $\alpha(\hbar\omega-E_g)$ is the step function denoting the density of states, and $f_e(\hbar\omega)$ and $f_h(\hbar\omega)$ are the Fermi distributions for electrons and holes. For nondegenerate systems the distribution function becomes simply the Boltzmann distribution. If the temperature of the electrons and holes are assumed to be equal, then the intensity reduces to

$$I(\hbar\omega)\propto\alpha(\hbar\omega-E_g)e^{-(\hbar\omega-E_G)/k_BT}. \tag{2}$$

One can see from Eq. (2) that the band-to-band luminescence is described by a simple exponential, the slope of which in a semilog plot provides a direct measurement of the carrier temperature.

Figure 2 is a comparison of the experimental absorption spectrum with the PL spectrum. In Fig. 2(a), the two lowest-

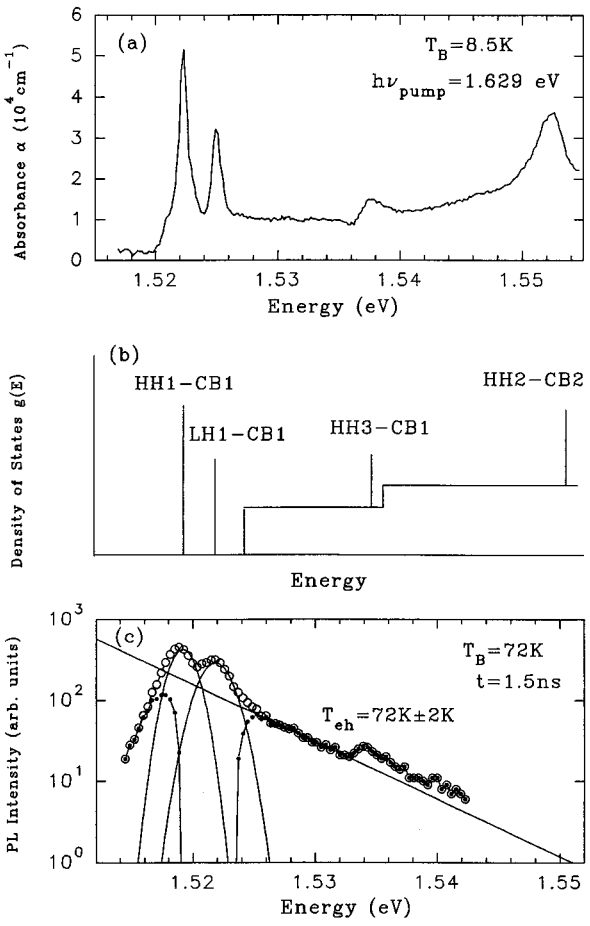

FIG. 2. (a) Absorbance spectrum of the GaAs quantum well. (b) Diagram of the exciton and electron-hole band-to-band density of states (DOS). (c) Semilogarithmic plot of the PL spectrum taken at $T_{\mathrm{Bath}}=72$ K. The curves are Gaussian fits to the exciton luminescence, and the line shows the slope of the band-to-band recombination, giving $T_{e\text{-}h}=72$ K.

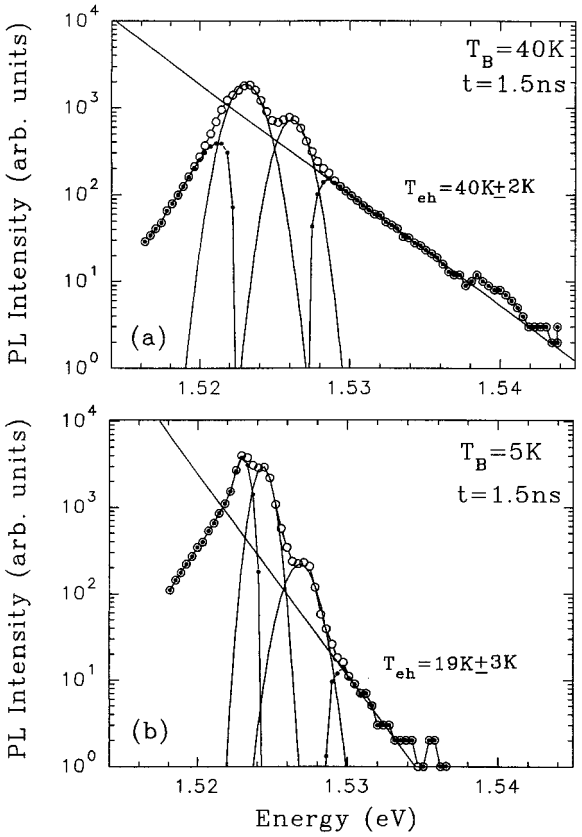

FIG. 3. PL spectra taken at (a) $T_{\mathrm{Bath}}=40$ K, and (b) 8.5 K. The Gaussians are fits to the heavy- and light-hole excitons. The temperatures measured from the slope of the band-to-band recombination are shown.

energy features in the absorption spectrum are the heavy- and light-hole exciton absorption peaks. The higher features are due to excitonic resonances composed of (1) a hole in the third heavy-hole valence band and an electron in the first confined conduction band (HH_3-CB_1), and (2) a hole in the second heavy-hole valence band and an electron in the second confined conduction band (HH_2-CB_2).[22] Figure 2(b) is a diagram with the absorbance of excitons shown as δ functions in energy, and the absorbance of the band-to-band recombination shown as step functions in energy. Figure 2(c) is the PL spectrum of the same sample taken at $T_{\mathrm{Bath}}=72$ K. The heavy- and light-hole excitons are fitted by Gaussians, and the fitted Gaussians are subtracted from the PL spectrum in order to isolate the luminescence arising from the band-to-band recombination. We see that the measured temperature from the electron-hole (eh) recombination of 72 ± 2 K is essentially the same as that measured by an external temperature sensor mounted on the sample probe.

To further confirm that the temperatures measured from T_{eh} accurately reflect the carrier temperatures, the PL spectra at different T_{Bath} are measured. Figure 3 shows the plot of the PL spectra at 40 and 5 K for excitation with an excess energy of 67 meV. The spectra are taken at 1.5 ns after the pump pulse. We see that the band-to-band PL is separated in energy from the heavy-hole exciton by the binding energy of $\sim$6 meV. This measured binding energy is in close agreement with the calculated value,[20] 6.2 meV for a GaAs quantum well with $L_Z=210$ Å . The low-energy feature below the

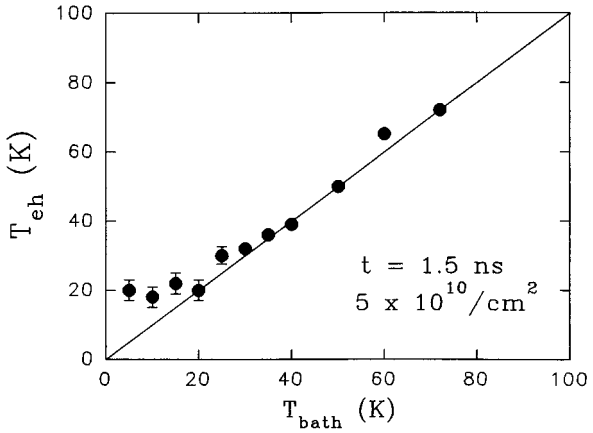

FIG. 4. The temperatures derived from the high-energy tail of the luminescence at $t=1.5$ ns after the excitation. The bath temperatures are measured with a silicon diode sensor attached to the sample mount.

heavy-hole exciton energy is due to excitons bound to defects. In Fig. 4, we plot the spectroscopic temperatures determined from the band-to-band luminescence. For bath temperatures above $\sim$30 K the carrier temperatures at 1.5 ns are equal to the bath temperatures, but, below 30 K, T_{eh} remains above the bath temperature. The source of this elevated temperature is not determined in our study.

The time dependence of the carrier temperatures is obtained from a series of time-resolved PL spectra. Two examples of the temperature decay are shown in Fig. 5, which shows the PL spectra at $T_{\mathrm{Bath}}=40$ K and an excitation energy equal to 67 meV at 33 ps and 1.82 ns. The spectra show that excitation with energies in excess of the heavy-hole energy leads to the formation of ''hot'' carriers with temperatures greater than the lattice temperatures. In Figs. 6(a) and 6(b) we show the time dependence of the carrier temperature for 45- and 38-meV excess energies. At early times just after the excitation, the carrier temperature reaches nearly 200 K, which is far above the bath temperature of 40 K, and cools to the lattice temperature in less than 0.5 ns. The carrier cooling can be well fitted by a single-exponential curve with a time constant of 44 ps, which is very near our instrumental resolution of 36 ps.

We see in Fig. 6(b) that, at a bath temperature of 8.5 K, the time evolution of the carrier temperatures is more complicated than at $T_{\mathrm{Bath}}=40$ K. The cooling curve is not a single exponential, and has a substantially slower component that remains beyond 2 ns which requires two additional exponential terms to reasonably represent the time-dependent behavior. The slower relaxation to the bath temperature is also implicit in Fig. 4 where, for bath temperatures below $\sim$20 K, the measured carrier temperature at 1.5 ns remains near 20 K instead of quickly reaching the bath temperature. As can be seen from Fig. 3(b), it is difficult to determine carrier temperatures much below 20 K.

The temperatures measured from nonresonant excitation pump energies at bath temperatures of 40 and 8.5 K show a fast initial temperature decay with a $\sim$44-ps time constant. The fast cooling is presumably due to the LO-phonon-mediated energy relaxation. Above 40 K there is still a significant fraction of carriers with energy greater than the LO-

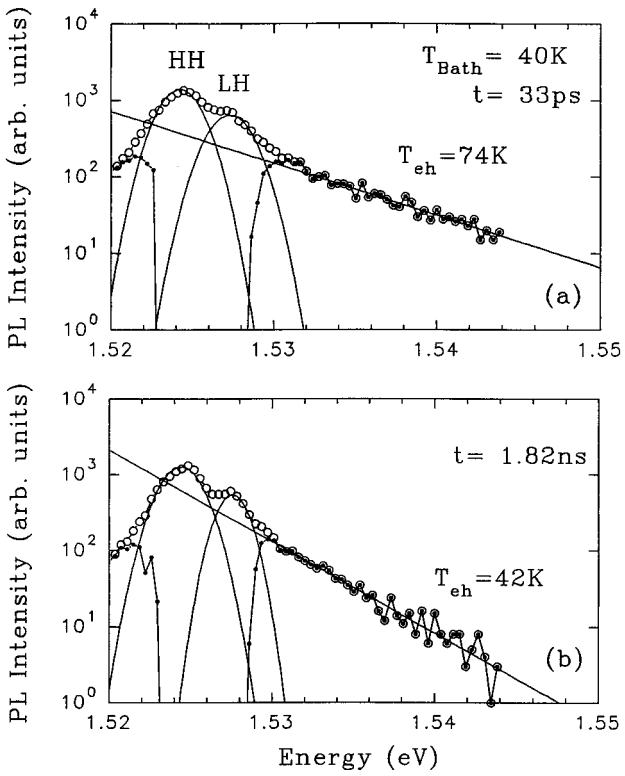

FIG. 5. PL spectra shown for (a) $t=33$ ps and for (b) $t=1.82$ ns after the excitation pulse. The labeled features are the heavy- and light-hole-exciton PL and the temperature is obtained from a fit of the high-energy tail to a single exponential.

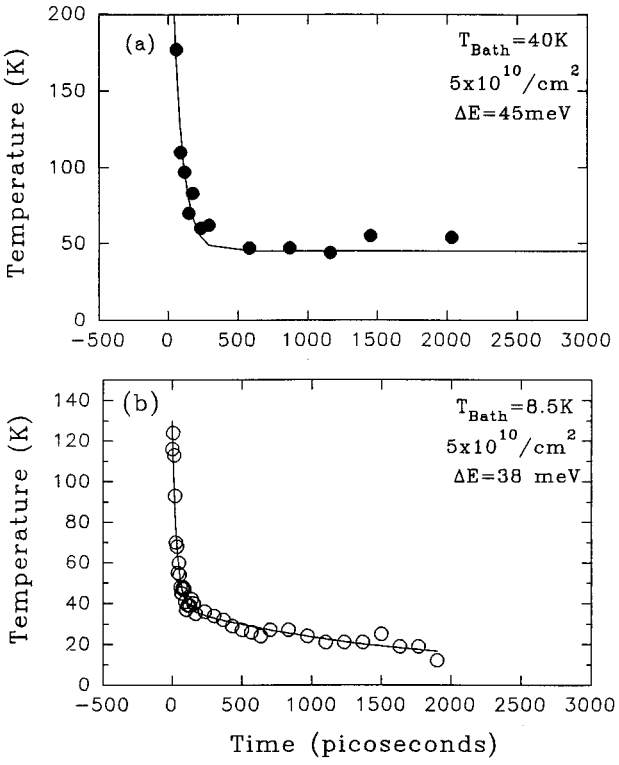

FIG. 6. (a) The carrier temperatures measured from the high-energy tail with the bath temperature at 40 K and an excitation energy of 45 meV above the heavy hole energy. (b) Carrier temperatures with the bath temperature at 8.5 K and an excess energy of 38 meV. The curves through the data are fits to Eq. (16), as described in the text.

phonon energy, so that the fast decay channel is available to the carriers. As the carriers cool at $T_{\mathrm{Bath}}=40$ K, there is no slowing down of the temperature decay as observed at $T_{\mathrm{Bath}}=8.5$ K. It has been shown in other studies that, for $T\geqslant 40$ K, energy loss of carriers occurs through the fast LO-phonon channel, but, as the carrier temperature falls below ~ 40 K, the small fraction of carriers above the LO-phonon energy is less important to carrier cooling than the slower but heavily populated acoustic-phonon-mediated channel.[23] The slower cooling rate found in Fig. 6(b) is thus attributed to acoustic-phonon emission. The acoustic-phonon relaxation behavior is nonexponential, but we find it useful to represent empirically the time dependence of the temperature as two acoustical-phonon-related exponential terms, as discussed below in the context of Eq. (16).

Figure 7 shows both the experimental energy-loss-rate curves derived from fitted functions of the experimental data in Figs. 6(a) and 6(b) along with the calculated LO-phonon-mediated energy-loss rate and the acoustic-phonon-mediated energy-loss rates. The mean energy loss per carrier due to LO-phonon emission in bulk GaAs is[24]

$$\left\langle \frac{dE}{dt}\right\rangle_{\mathrm{LO}}\left(\frac{eV}{s}\right)=1.27\times 10^{12}\left(\frac{m^*}{m_0}\right)^{1/2}\exp\left[-\frac{\hbar\omega_{\mathrm{LO}}}{k_B T_{\mathrm{eh}}}\right]. \quad (3)$$

To calculate the LO-phonon-mediated cooling rate, we use the heavy-hole effective mass $0.45m_0$. Since the effective mass of the holes is larger than the electrons by a factor of 6, carrier cooling occurs primarily through hole cooling.[25]

Cooling by acoustic-phonon emission occurs through deformation-potential scattering and piezoelectric scattering. Goebel[24] calculated both contributions, and deformation-potential cooling by acoustic-phonon emission for a Boltzmann carrier distribution in bulk GaAs is given by

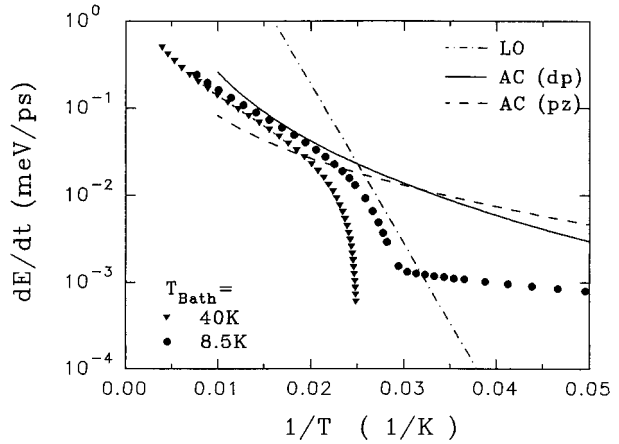

FIG. 7. Plot of the fitted functions of the experimentally measured cooling curves from Figs. 6(a) and 6(b) at bath temperatures at 40 K (filled triangles) and at 8.5 K (filled circles). The dot-dashed line is the energy-loss rate derived using LO-phonon-mediated cooling. The AC-phonon-mediated energy-loss rate by deformation potential and piezoelectric is shown by solid and dashed curves, respectively.

$$\left\langle \frac{dE}{dt} \right\rangle_{dp} \left(\frac{eV}{s} \right) = 7.88 \times 10^5 \left(\frac{m^*}{m_0} \right)^{5/2} \left(\frac{k_B T_{\rm eh}}{\rm meV} \right)^{3/2} \times \frac{(T_{\rm eh} - T_{\rm Bath})}{T_{\rm eh}}. \quad (4)$$

The piezoelectric scattering is given by

$$\left\langle \frac{dE}{dt} \right\rangle_{\rm pz} \left(\frac{eV}{s} \right) = 1.18 \times 10^7 \left(\frac{m^*}{m_0} \right)^{3/2} \left(\frac{k_B T_{\rm eh}}{\rm meV} \right)^{1/2} \times \frac{(T_{\rm eh} - T_{\rm Bath})}{T_{\rm eh}}, \quad (5)$$

using the piezoelectric modulus of GaAs, 4.8×10^{14} cm^{-1} g$^{1/2}$s^{-1}. The acoustic-phonon energy-loss rate due to the deformation potential and piezoelectric scattering are also plotted in Fig. 7. We see that our experimentally measured curves reproduce the basic features of the predicted energy-loss-rate curves for bulk GaAs. However, we see (and others have also found) that the experimentally measured cooling rates are smaller than those predicted for bulk GaAs.[16] The discrepancy between the measured and the predicted cooling has been attributed to the reduction in the energy-loss rate by screening and the generation of nonequilibrium phonons.[3]

THERMODYNAMICS OF THE EXCITONIC GAS

The simultaneous luminescence of excitons and free carriers in a quantum well raises the possibility that the two species are in thermodynamic equilibrium. This would imply both thermal and chemical equilibria, whereby the relationship between the exciton population and the carrier population is given by[17]

$$[e] + [h] \overset{E_B}{\leftrightarrow} [ex]. \quad (6)$$

Here $[e]$ is the electron density n_e, $[h]$ the hole density n_h, $[ex]$ the exciton density $n_{\rm ex}$, and E_B the exciton binding energy. The densities are related through a temperature-dependent equilibrium constant n^* as follows:

$$\frac{n_e n_h}{n_{\rm ex}} = n^*, \quad (7)$$

where n^* is given by

$$\ln n^* = -\ln n_Q({\rm ex}) + \ln n_Q(e) + \ln n_Q(h) - E_B/k_B T. \quad (8)$$

In this equation, n_Q is a quantum concentration in two dimensions given by, for example,

$$n_Q(e) = \frac{m_e k_B T}{2\pi\hbar^2}. \quad (9)$$

With the respective effective masses, n^* becomes

$$n^* = \frac{k_B T}{2\pi\hbar^2} \frac{m_e m_h}{m_{\rm ex}} e^{-E_B/k_B T} \text{ where } m_{\rm ex} = m_e + m_h. \quad (10)$$

With the substitution of the effective masses $m_e = 0.066 m_0$ and $m_h = 0.45 m_0$, n^* is evaluated as

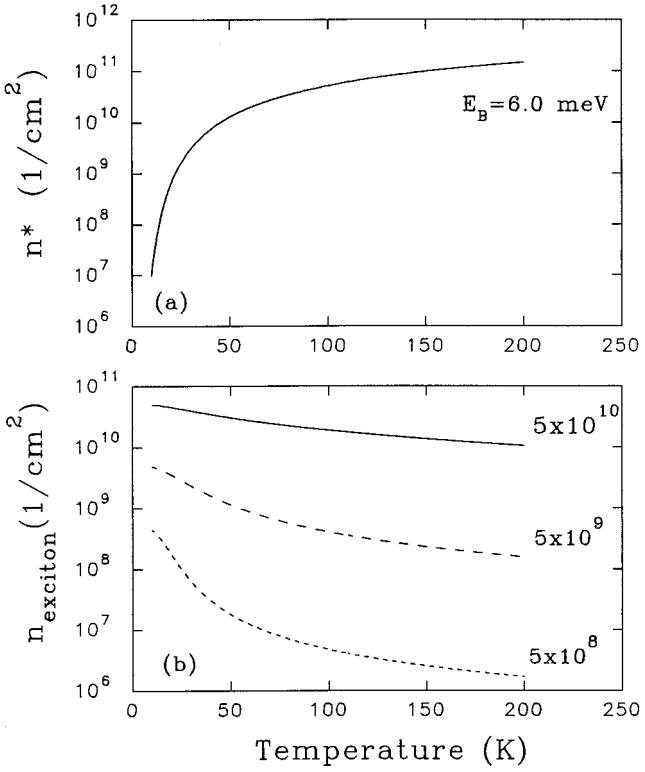

FIG. 8. (a) Plot of n^* as a function of temperature using $E_B = 6$ meV, an electron effective mass of $0.0665 m_0$, and a hole effective mass of $0.45 m_0$. (b) Plot of $n_{\rm ex}$ for various values of N, the total carrier density, in units of cm^{-2}.

$$n^* = k_B T \frac{1.215 \times 10^{10}}{\rm meV\ cm^2} e^{-E_B/k_B T}, \quad (11)$$

where $k_B T$ is given in meV. Figure 8(a) shows a plot of n^* as a function of temperature with the binding energy, $E_B = 6.0$ meV.

In our experiments we employ picosecond excitation pulses that are much shorter than the exciton or carrier lifetimes; thus we assume that the total number of electron-hole pairs produced are equal to the number of absorbed photons. Hence, if the volume occupied by the carriers is determined, we can determine the initial total carrier density N. A relationship between N and the exciton density needs to be established from the thermodynamic relations. Substitution of $n_e = N - n_{\rm ex}$ into Eq. (7) results in a quadratic equation for $n_{\rm ex}$. Therefore, the total exciton concentration as a function of incident photon density is given by

$$n_{\rm ex} = \left[\frac{-\sqrt{n^*} + \sqrt{n^*}\left(1 + \frac{4N(t)}{n^*} \right)^{1/2}}{2} \right]^2, \quad (12)$$

choosing the $(+)$ sign because as N goes to zero, $n_{\rm ex}$ must go to zero. Figure 8(b) shows a plot of Eq. (12) for various total carrier densities N.

Since the excitonic state is composed of an electron and a hole, it is described by an energy-momentum relation different from that of the separate carrier states. Excitons can recombine only near $k = 0$ due to the conservation of momen-

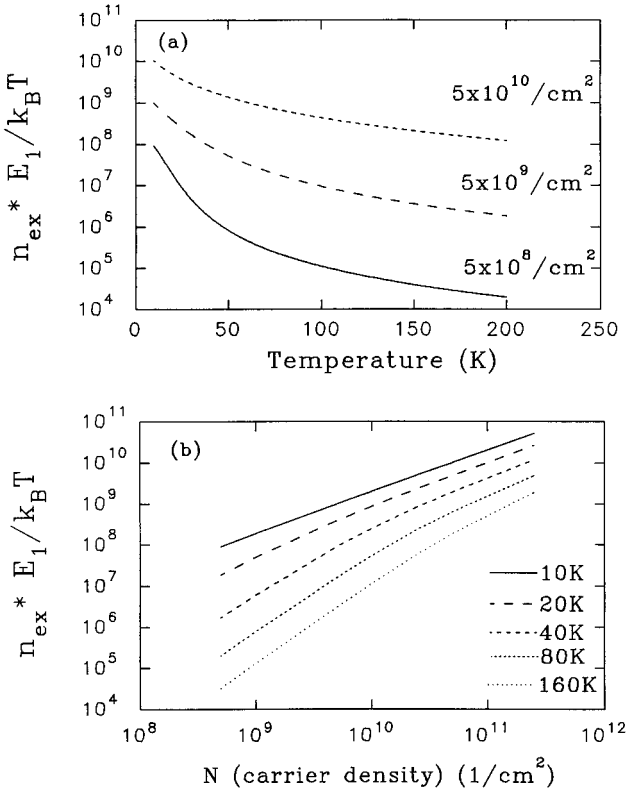

FIG. 9. (a) Plot of $n_{ex}E_1/k_BT$, the number of excitons which can emit a photon vs temperature. (b) Number of excitons which can couple to photons vs the initial excited carrier density.

tum, in practice given by a finite spectral width E_1, defined by the energy crossing of the photon and exciton dispersion curves above the exciton band bottom. E_1 is typically ~ 0.1 meV in GaAs structures.[1] The radiative recombination of excitons occurs within a homogeneous width Γ_h which in principle can be greater or less than E_1, but is typically somewhat larger in magnitude.[26] In this limit, the PL intensity is given by[18]

$$I(T(t),t)=An_{ex}(T(t),t)\frac{E_1}{3\hbar\Gamma_h}(2\Gamma_0)(1-e^{-\hbar\Gamma_h/k_BT(t)}), \tag{13}$$

where Γ_0 is the fundamental radiative recombination rate, and A is the area of the quantum well. The homogeneous width varies with both temperature and density.[27] However, one can see from Eq. (13) that if the kinetic energy of carriers is greater than the homogeneous width, then the equation reduces to

$$I(T(t),t)=An_{ex}(T(t),t)\frac{E_1}{3k_BT(t)}(2\Gamma_0). \tag{14}$$

Shown in Fig. 9(a) is a plot of the right side of Eq. (14) as a function of temperature for various total carrier densities N. We see from a comparison to Fig. 8(b), that the additional temperature term has a significant effect on the predicted exciton intensity. In Fig. 9(b), we plot the right side of Eq. (14) versus the total carrier density at various temperatures. At 10 K, the excitons and the total carriers have a linear relationship, indicating that all the carriers exist as excitons. At higher temperatures, a curvature at low densities is seen, indicating the predominance of free electrons and holes over excitons.

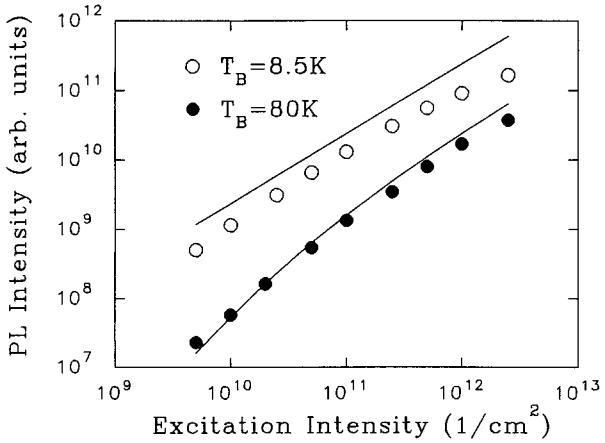

FIG. 10. The calculated number of excitons vs the total carrier density plotted with the experimentally measured time-integrated exciton intensity. At 80 K, the increasing curvature at low densities is due to the loss of excitons to the exciton ionization into free electrons and holes.

We may now compare the experimental time-integrated exciton luminescence with the above model. The number of excitons which can couple to photons is a function of both the incident photon density and the temperature. Figure 10 shows the experimentally measured time-integrated exciton intensities and a plot of the right side of Eq. (14) as a function of density at two bath temperatures. At 8.5 K, all the carriers are converted to excitons, while at 80 K there is a deviation away from a straight line due to entropy ionization at the lowest density, as predicted by our analysis. The deviation of the data from a linear behavior at high densities and 8.5 K is not accounted for.

TIME EVOLUTION OF EXCITONIC LUMINESCENCE

From the previous analysis of the time evolution of the carrier density and the carrier temperature and Eq. (13), we can attempt to fit the time dependence of the exciton luminescence intensity. We use the temperatures reported in the earlier part of this work, and the spatial measurements reported in our previous work.[15] The recombination decay of carriers and the decrease in density due to spatial expansion are taken into account by using

$$N(t)=N_0e^{-t/\tau_D}\frac{\Delta_0^2}{\langle\Delta^2(t)\rangle}. \tag{15}$$

The recombination time τ_D is found by a fit to data, and the decrease in the carrier density due to spatial expansion is accounted for by the increase in the square of the spatial full width at half-maximum, $\Delta^2(t)$.

Figure 11(a) shows a fit of the excitation luminescence using the fit to the temperatures in Fig. 11(b) along with the spatial expansion of the carriers shown in Fig. 11(c). The

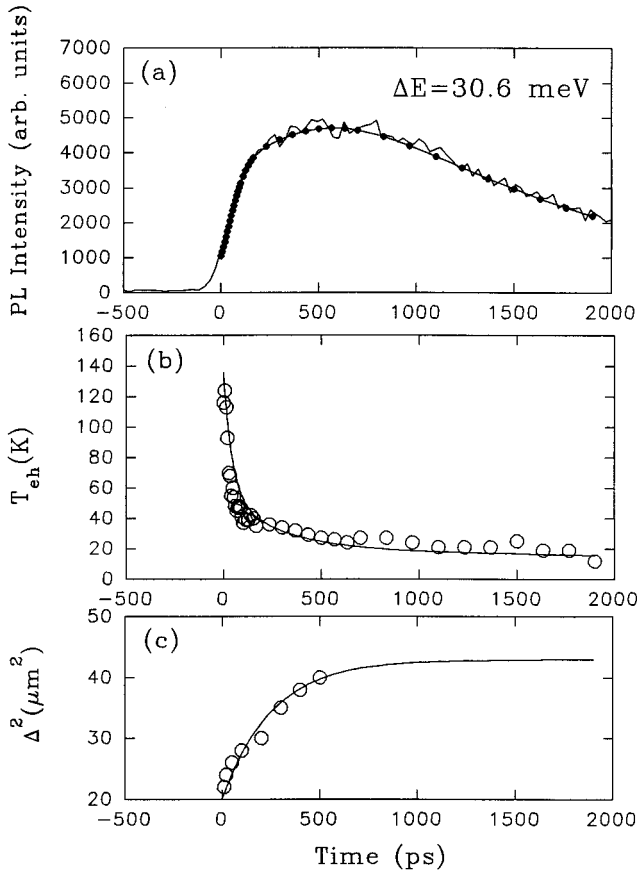

FIG. 11. (a) Dots are a fit of the experimental exciton luminescence profile (solid curve) by the model described in the text. (b) The solid curve is Eq. (16) fit to the experimental carrier temperatures (circles). (c) The solid curve is Eq. (17) fit to the experimental expansion data (circles).

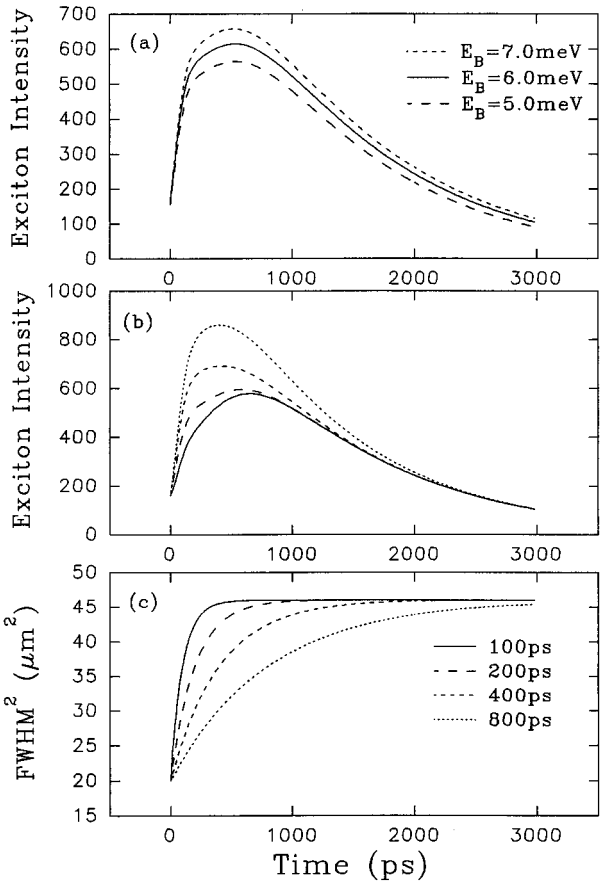

FIG. 12. (a) Simulation of the luminescence intensity for various excitonic binding energies. (b) Simulation of the luminescence intensity for the spatial expansion rates listed in (c). (c) Simulation of the expansion using Eq. (17) under various expansion time constants.

temperatures used in the fit are taken from a three-exponential fit of the experimentally measured temperatures as in Fig. 6(b),

$$T(t)=T_0(a_1e^{-t/\tau_1}+a_2e^{-t/\tau_2}+a_3e^{-t/\tau_3}). \tag{16}$$

Although the three exponential terms are merely an empirical representation of the time dependence of the measured temperature, physically the fast τ_1 term is due to LO-phonon cooling, and the latter two terms are due to slower acoustical-phonon relaxation.

In Eq. (16), the parameter T_0 is set equal to 130 K, and τ_1, τ_2, and τ_3 are found to be 45, 281, and 4305 ps, respectively. The coefficients a_1, a_2, and a_3 equal 0.625, 0.281, and 0.094, respectively. The particular temperature function is chosen to closely parallel the temperature dependence observed experimentally in Fig. 6(b).

The spatial expansion of carriers is modeled by a function which closely mirrors the actual data,[15]

$$\Delta^2(t)=\Delta_c^2(1-e^{-t/\tau_{\rm exp}})+\Delta_0^2. \tag{17}$$

Figure 11(c) shows a fit of this function to the experimentally measured Δ^2 with Δ_c^2 and Δ_0^2 equal to 23 and 20 μm^2 respectively, and $\tau_{\rm exp}$ equal to 255 ps.

We can now adjust the various parameters of the model to isolate the effects of the various physical processes. The purpose is to gain insights which may be applicable to systems other than the particular sample studied here. In the following analysis, we examine the effects of changing E_B and the rate of spatial expansion on the fitted luminescence profile in Fig. 11(a).

Figure 12(a) shows a plot of the calculated exciton PL for $E_B=5.0$, 6.0, and 7.0 meV. This analysis shows that the basic shape of the profile is not affected by changes in the binding energy over this range. The only change is the increase in the intensity beyond $\sim$100 ps as the binding energy is increased. The result is easily understood because the greatest effect from the changes in binding energy occurs at low $T_{\rm eh}$. The increase in the binding energy means that more carriers exist as excitons instead of free electrons and holes, and thus the exciton PL intensity increases.

More drastic changes occur by varying the rate of spatial expansion. Figure 12(c) shows a plot [Eq. (17)] as a function of time for various expansion time constants, $\tau_{\rm exp}$. The initial diffusivities in Fig. 12(c) range from $\sim$180 to $\sim$20 cm^2/s, which is close to the range of previously measured initial diffusivities.[15] Figure 12(b) shows the effect of the change in the spatial expansion rate on the time-resolved exciton PL. In Fig. 12(b), only the expansion time constant

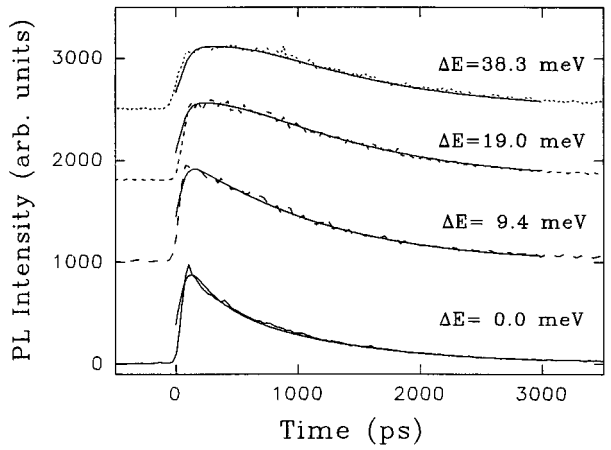

FIG. 13. Data and model fits (smooth curves) of the exciton luminescence profiles for varying excess energy, $\Delta E = \hbar\omega_{\text{laser}} - E_{\text{HH}}$.

was changed. The two main effects of increasing the rate of expansion are (1) the peak of the time-resolved intensity moves to later time, and (2) the initial dI_{ex}/dt decreases with faster expansion.

EXCESS ENERGY AND DENSITY DEPENDENCE OF THE EXCITON LUMINESCENCE

The primary motivating factor in undertaking these studies is to try to understand the excitonic temporal profile as a function of excess energy, $\Delta E = \hbar\omega_{\text{laser}} - E_{\text{HH}}$, as well as excitation density. The excess energy is not explicitly included in the equations for the temperature evolution, Eq. (16), or the spatial expansion, Eq. (17). We expect that the initial temperature will depend upon the excess energy. Also, we vary both Δ_c^2 and τ_{exp} in Eq. (17) to obtain the optimal fits to the data. The chosen values of these parameters closely reflect the actual time-resolved spatial measurements under similar conditions.[15] Due to the number of adjustable parameters, the fitting procedure is capable of only providing a plausible picture of the processes involved, not an accurate determination of the specific parameters.

Fits to the excitonic temporal profiles using this procedure for several values of excess energy are shown in Fig. 13, using the temporal distributions of carrier temperature and spatial volume plotted in Fig. 14. The parameters for the fits shown in Fig. 13 are shown in Table I [for these fits the value a_1 in Eq. (16) is set to 1]. The values of T_0 in Eq. (16) are found by measuring the time to the peak of the maximum exciton intensity as in Refs. 1 and 2. Thus T_0 increases from 34 K with near-resonant excitations to 130 K for $\Delta E = 34$ meV. In Fig. 13, we find that near-resonant excitation requires that the acoustical phonon relaxation terms [a_2 and a_3 in Eq. (16)] must be eliminated to obtain good fits to the data [see Fig. 14(a)]. This implies that acoustical-phonon relaxation is not an important aspect in a description of our data for the near-resonant excitation case. This is physically reasonable because, with the carriers much cooler from the start, acoustical-phonon emission is not expected to play as strong a role in the dynamics.

The carrier density dependence at a fixed excess energy

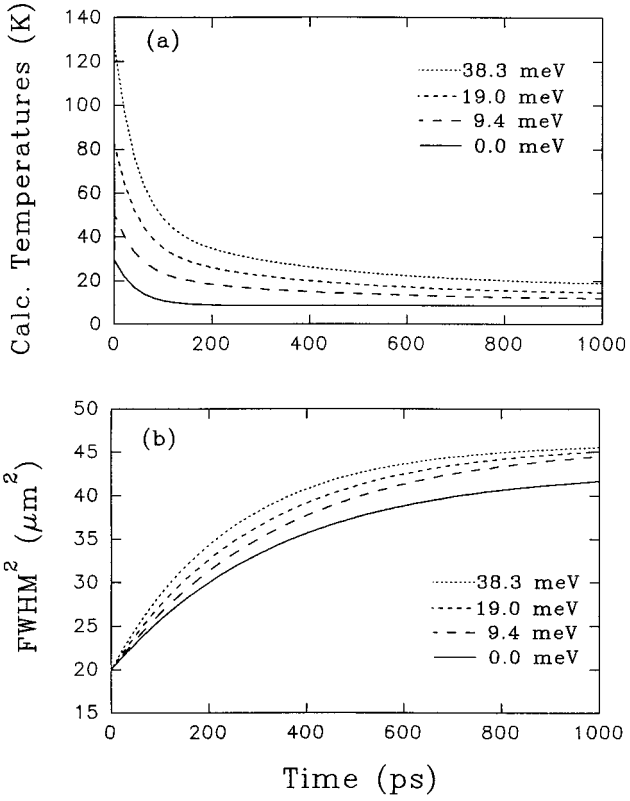

FIG. 14. (a) Carrier temperatures used in the fits of Fig. 13. (b) Δ^2 vs time used in the fits of Fig. 13.

can be treated by a similar procedure. We saw in Fig. 1 that excitation with a constant photon energy and increasing density causes major changes in the temporal profile of the exciton PL. We noted that as the excitation density is increased, the time at which the signal reaches a peak intensity occurs progressively at later times. Accordingly, the temporal full width at half-maximum becomes wider with increasing excitation density.

Using Eqs. (14), (16), and (17), we are able to obtain very good fits to the time-resolved exciton PL intensity by adjusting the time-dependent temperatures and the spatial expansion. The principal results are shown in Fig. 15. The parameters for the fits shown Fig. 15 are shown in Table II [the value a_1 in Eq. (16) is again set to 1]. The temperature dependencies obtained in these fits are given in Fig. 16(a), and the corresponding Δ^2 vs time that account for spatial expansion are shown in Fig. 16(b). The temperature dependencies are found by using Eq. (16).

TABLE I. Parameters used in the fits shown in Fig. 13.

Excess energy (meV)	T_0 (K)	a_2	a_3	τ_D (ps)	Δ^2	τ_{exp} (ps)	A (cm^2)
0	34	0.0	0.0	1050	23	350	1.6×10^{-7}
9.4	43	0.45	0.15	1000	26	350	8.2×10^{-8}
19.0	75	0.45	0.15	1100	26	300	1.1×10^{-7}
38.3	130	0.35	0.15	1100	26	250	1.5×10^{-7}

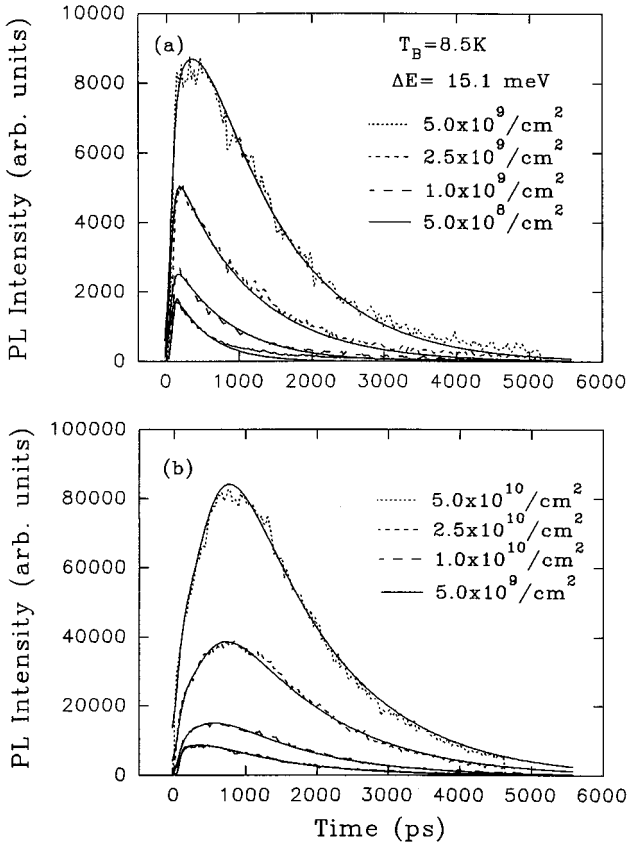

FIG. 15. (a) Time-dependent data and model fits (smooth curves) of the heavy-hole exciton PL at excitation densities from $5\times10^8/\mathrm{cm}^2$ to $5\times10^9/\mathrm{cm}^2$. (b) Same for excitation densities from $5\times10^9/\mathrm{cm}^2$ to $5\times10^{10}/\mathrm{cm}^2$.

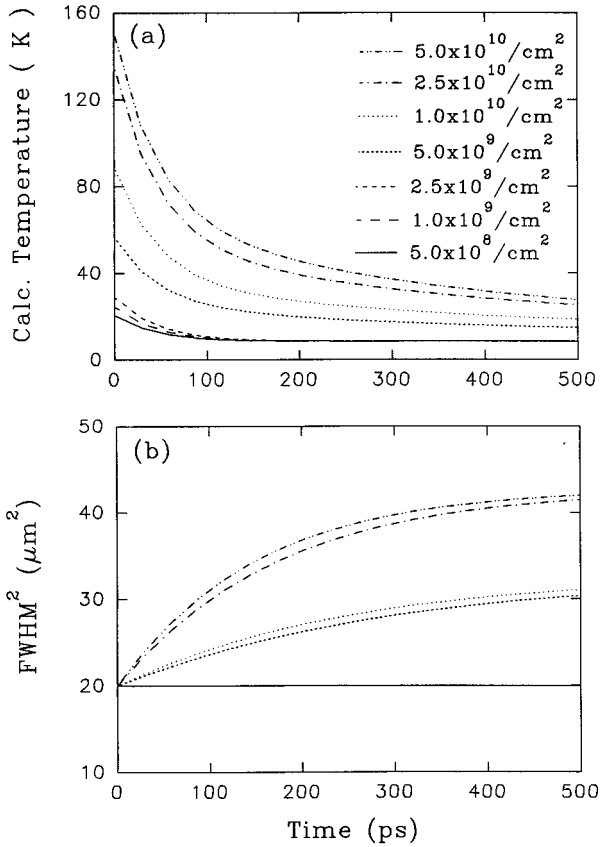

FIG. 16. (a) Carrier temperatures used in the fits of Fig. 15. (b) Spatial full widths at half maxima used in the fits of Fig. 15.

DISCUSSION AND SUMMARY

An important result of our analysis is that the initial carrier temperature increases as a function of both carrier density and excess energy. Figure 17(a) shows the initial temperatures T_0, derived from the first as a function of excess energy. The open squares denote the experimentally measured temperatures, obtained only for the extreme values of excess energy, and the solid circles denote the fitted temperatures for intermediate values of excess energy.

The heating of the carriers with increased excess energy seems reasonable, but the details require some thought. Carriers are created by the laser pulse with an average kinetic energy equal to $\hbar\omega_{\mathrm{laser}}-E_{\mathrm{HH}}$. In two-dimensional systems, the temperature related to this average kinetic energy for a Boltzmann distribution is $\langle E\rangle=k_BT$. The initial temperatures calculated in this way are generally far above the 100 K or so observed in our measurements. This is because carrier cooling due to LO-phonon emission reduces the carrier temperatures on a subpicosecond scale, considerably shorter than our time resolution and earliest well-defined observation time. One might expect that the carrier temperatures measured after the LO-phonon relaxation process occurs would reach some fraction of the LO-phonon energy, which is only weakly dependent on the initial carrier temperature.

TABLE II. Parameters used in the fits shown in Figs. 15(a) and 15(b).

Density (/cm^2)	T_0 (K)	a_2	a_3	τ_D (ps)	Δ^2	τ_{exp} (ps)	A (cm^2)
5.0×10^8	23	0.0	0.0	500	0.0		5.5×10^{-6}
1.0×10^9	30	0.0	0.0	800	0.0		3.6×10^{-6}
2.5×10^9	38	0.0	0.0	1050	0.0		2.7×10^{-6}
5.0×10^9	52	0.45	0.15	1100	12.8	300	9.0×10^{-6}
1.0×10^{10}	95	0.45	0.15	1200	12.8	250	9.5×10^{-6}
2.5×10^{10}	144	0.50	0.15	1250	22.8	175	20×10^{-6}
5.0×10^{10}	150	0.63	0.15	1210	22.8	150	22×10^{-6}

Nevertheless, the results shown in Fig. 17(a) are in qualitative agreement with previous work by Goebel and Hildebrand.[24] In their work, they show that under continuous wave (cw) excitation, at $T_{\mathrm{Bath}}=2$ K, the plasma temperatures measured from the high-energy slope of the photoluminescence spectra increase from 10 to 50 K as the excess energy increases from 5 to 40 meV. Under cw excitation, they were sensing a time-averaged temperature; thus we expect their measured temperatures to be lower than our initial time-resolved temperatures.

The answer to this puzzle of elevated temperatures may be similar to that proposed by Shah and Leite,[28] who made similar measurements for bulk GaAs using cw argon-ion laser excitation. They too observed an increase in the carrier temperatures with excitation density. At high densities they found that the measured carrier temperature was related to the excitation intensity by $I\propto(-\hbar\omega_{\mathrm{LO}}/k_BT_e)$. They viewed the carrier system as composed of (1) the hot carriers created

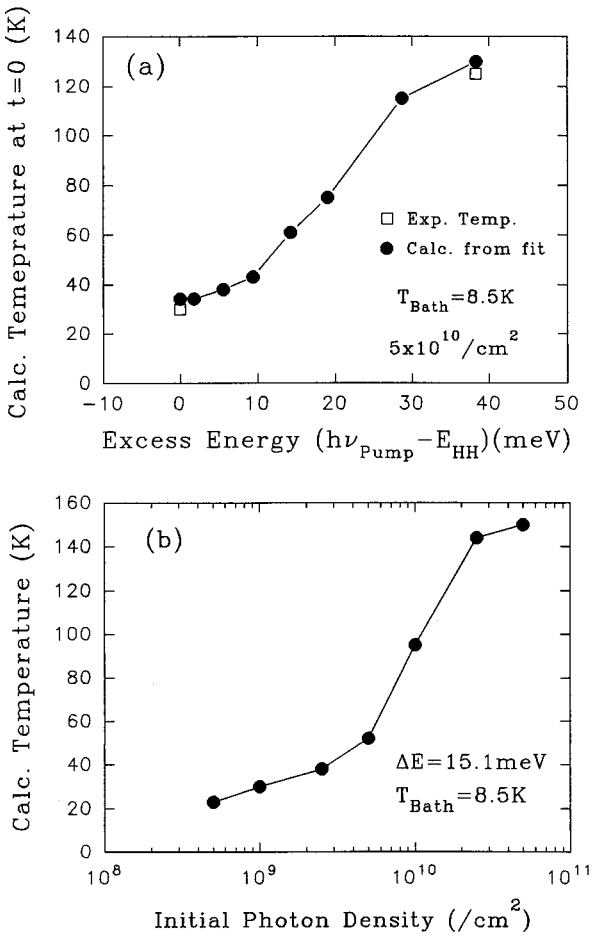

FIG. 17. (a) Initial temperatures plotted from Fig. 14(a) vs the excitation energy. (b) Initial temperatures plotted from Fig. 16(a) vs the initial photon densities.

by the excitation, and (2) the cooler carriers which had already lost most of their excess energy and were responsible for the PL.[29] If the total density of the carriers is high enough, the hot carriers could bypass the LO-phonon-emission process and lose most of their excess energy by scattering with the reservoir of colder carriers. In this way, the colder-carrier distribution would be heated at higher excitation densities. This heating is offset by emission of LO phonons in the tail of the colder-carrier distribution, leading to the dependence stated above.

How does this idea fit our data? In Fig. 18, we have plotted the inverse carrier temperature versus the initial absorbed photon density. At high density the data follow along the straight line corresponding to the LO-phonon energy of 36

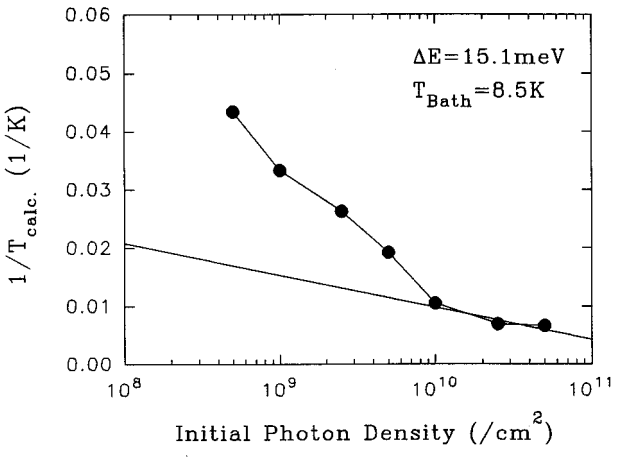

FIG. 18. Inverse of the calculated temperatures plotted vs initial photon intensities. The straight line has a slope given by the LO-phonon energy of 36 meV.

meV, in agreement with Shah and Leite's observations and with the relationship described in the last paragraph. As they found, we see that at low densities the dependence is weaker than that given by the exponential line. Apparently some other energy-loss mechanisms are becoming operative in this low-temperature/low-density regime.

In summary, our measurements and analysis show that the temporal profiles of excitonic photoluminescence following pulsed excitation of a GaAs quantum well can be understood in terms of a gas of excitons in thermal and chemical equilibrium with free carriers. Because localized excitation is used to produce high gas densities, it is necessary to take into account the changing volume of the excitonic cloud as well as the evolution of the gas temperature. The carrier temperatures were obtained from the slopes of the band-to-band PL spectra, and the carrier cooling rates were in agreement with the expected LO- and acoustic-phonon emission rates. Our analysis showed interesting dependencies of the carrier temperatures on the excess energy induced by the laser photons and on the carrier densities. These latter results are in qualitative accord with earlier results for cw excitation and bulk GaAs.

ACKNOWLEDGMENTS

This work was supported by the Department of Energy under the MRL Grant No. DEAC02-76ER01198. The experiments were performed in the Laser Laboratory Facility of the Materials Research Laboratory.

*Present address: Dept. of Physics, Dartmouth College, Hanover, N.H. 03755.

[1] A. Vinattieri, Jagdeep Shah, T. C. Damen, D. S. Kim, L. N. Pfeiffer, M. Z. Maialle, and L. J. Sham, Phys. Rev. B **50**, 10 868 (1994).

[2] *Hot Carriers in Semiconductor Nanostructures, Physics and Applications*, edited by J. Shah (Academic, New York, 1992).

[3] K. Kash, J. Shah, D. Block, A. C. Gossard, and W. Wiegmann, Physica **134B**, 189 (1985).

[4] W. H. Knox, D. S. Chemla, G. Livescu, J. Cunningham, and J. E. Henry, Phys. Rev. Lett. **61**, 1290 (1988).

[5] J. Kusano, Y. Segawa, Y. Aoyagi, S. Namba, and H. Okamoto, Phys. Rev. B **40**, 1685 (1989).

[6] Ph. Roussignol, C. Delalande, A. Vinattieri, L. Carraresi, and M. Colocci, Phys. Rev. B **45**, 6995 (1992).

[7] R. Eccleston, R. Strobel, W. W. Rühle, J. Kuhl, B. F. Feuerbacher, and K. Ploog, Phys. Rev. B **44**, 1395 (1991).

[8] T. C. Damen, J. Shah, D. Y. Oberli, J. E. Cunningham, and J. M.

Kuo, Phys. Rev. B **42**, 7434 (1990).
[9] J. Feldmann, G. Peter, E. O. Gobel, P. Dawson, K. Moore, C. Foxon, and R. J. Elliot, Phys. Rev. Lett. **59**, 2337 (1987).
[10] P. L. Gourley and J. P. Wolfe, Phys. Rev. B **20**, 3319 (1979).
[11] J. C. Kim, D. R. Wake, and J. P. Wolfe, Phys. Rev. B **50**, 15 099 (1994).
[12] W. Picken and J. P. R. David, Appl. Phys. Lett. **56**, 268 (1990).
[13] B. K. Ridley, Phys. Rev. B **41**, 12 190 (1990).
[14] M. Colocci, M. Gurioli, and A. Vinattieri, J. Appl. Phys. **68**, 2809 (1990).
[15] H. W. Yoon, D. R. Wake, J. P. Wolfe, and H. Morkoç, Phys. Rev. B **46**, 13 461 (1992).
[16] K. Leo, W. W. Rühle, and K. Ploog, Phys. Rev. B **38**, 1947 (1988).
[17] G. Bastard, *Wave Mechanics Applied to Semiconductor Heterostructures* (Halsted, New York, 1988), p. 271.
[18] D. S. Citrin, Phys. Rev. B **47**, 3832 (1993).
[19] J. Shah, Superlatt. Microstruct. **6**, 293 (1989).
[20] C. Priester, G. Allen, and M. Lannoo, Phys. Rev. B **30**, 7302 (1984).
[21] G. Bastard, *Wave Mechanics Applied to Semiconductor Heterostructures* (Ref. 17), p. 281.
[22] W. T. Masselink, P. J. Pearah, J. Klem, C. K. Peng, H. Morkoç, G. D. Sanders, and Y. C. Chang, Phys. Rev. B **32**, 8027 (1985).
[23] J. Shah and R. F. Leheny, in *Semiconductors Probed by Ultrafast Laser Spectroscopy*, edited by R. R. Alfano (Academic, New York, 1984), Vol. I, p. 55.
[24] E. O. Goebel and O. Hildebrand, Phys. Status Solidi B **88**, 645 (1978).
[25] K. Leo, W. W. Rühle, and K. Ploog, Phys. Rev. B **38**, 1947 (1988); J. Shah, A. Pinczuk, A. C. Gossard, and W. Wiegmann, Phys. Rev. Lett. **54**, 2045 (1985).
[26] A. Honold, L. Schultheis, J. Kuhl, and C. W. Tu, in *Ultrafast Phenomena VI*, edited by T. Yajima, K. Yoshihara, C. B. Harris, and S. Shinoya, Springer Series in Chemical Physics Vol. 48 (Springer-Verlag, Berlin, 1988), p. 307.
[27] L. Schultheis, A. Honold, J. Kuhl, K. Köhler, and C. W. Tu, Phys. Rev. B **34**, 9027 (1986).
[28] Jagdeep Shah and R. C. C. Leite, Phys. Rev. Lett. **22**, 1304 (1969).
[29] Similar arguments have been applied in the study of ballistic phonons in silicon by M. E. Msall, S. Tamura, S. E. Esipov, and J. P. Wolfe, Phys. Rev. Lett. **70**, 3463 (1993); Sergei E. Esipov, M. E. Msall, and J. P. Wolfe, Phys. Rev. B **47**, 13 330 (1993).